Journal of Electron Spectroscopy and Related Phenomena 276 (2024) 147487

Contents lists available at ScienceDirect

Journal of Electron Spectroscopy and Related Phenomena

journal homepage: www.elsevier.com/locate/elspec

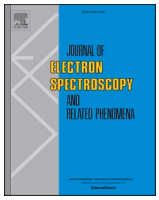

Comparison of soft X-ray spectro-ptychography and scanning transmission X-ray microscopy

Adam P. Hitchcock [a,*], Chunyang Zhang [a,b], Haytham Eraky [a], Drew Higgins [b], Rachid Belkhou [c], Nicolas Millle [c], Sufal Swaraj [c], Stefan Stanescu [c], Tianxiao Sun [d,1], Jian Wang [d]

[a] Chemistry & Chemical Biology, McMaster University, Hamilton, ON L8S4M1, Canada
[b] Chemical Engineering, McMaster University, Hamilton, ON L8S4M, Canada
[c] Synchrotron SOLEIL, L'Orme des Merisiers, Départementale 128, Saint-Aubin 91190, France
[d] Canadian Light Source, 44 Innovation Boulevard, Saskatoon, SK S7N 2V3, Canada

ARTICLE INFO

Keywords:
Scanning transmission X-ray microscopy, STXM
Spectro-ptychography
Cu nanoparticles
Cu 2p X-ray absorption

ABSTRACT

Over the past decade advances in instrumentation and software have enabled development of spectro-ptychography (SP) as a higher spatial resolution extension of scanning transmission X-ray microscopy (STXM). Direct comparisons are made of same-area chemical state imaging of Cu nanoparticles using STXM and SP in order to compare and contrast the two approaches. We show that SP gives very similar chemical state information as STXM with significantly better spatial resolution and much higher quality images and chemical maps, on account of finer pixels in the reconstructed images. When defocused spot sizes are used (i.e., 1–3 μm, as opposed to full-focus 30–50 nm) SP data acquisition is faster and the radiation dose delivered to the sample is smaller than the corresponding STXM measurement. The limitations of SP are primarily related to the time and complexity of the ptychographic reconstruction. We argue that these documented advantages mean that SP rather than STXM should be used for more complex studies such as tomography and *in situ* studies, especially when radiation damage is a concern. The main point of this manuscript is to illustrate, with scientifically relevant samples, the significant advantages of SP relative to conventional STXM, with the goal of encouraging greater use of SP.

1. Introduction

Over the past several decades, soft X-ray scanning transmission X-ray microscopy (STXM) has emerged as a powerful synchrotron-based spectro-microscopic technique for quantitative chemical characterization [1–5]. STXM provides X-ray imaging with high spatial resolution and sensitive chemical analysis. It provides morphological and chemical information of materials at the nano- and microscales. Chemical sensitivity is provided by near-edge X-ray absorption fine structure (NEXAFS) spectroscopy [6], the fine structure at core excitation edges. NEXAFS is sensitive to oxidation state, chemical functionality and bonding. It is also sensitive to geometric and magnetic anisotropy through linear and circular dichroism [2–4]. Electron energy loss spectroscopy (EELS) measured in a transmission electron microscope (TEM) [7,8] provides similar chemical sensitivity at much higher spatial resolution (<0.1 nm). Relative to TEM-EELS, STXM is particularly useful in studies of radiation sensitive systems, such as biological and polymer samples, due to its significantly lower radiation damage at comparable information rates, as compared to TEM-EELS [8–11].

STXM has seen extensive application in energy materials science [12–20] since it provides chemical and structural information beyond elemental identity, such as oxidation state, chemical bonding, coordination, orientation, and magnetic properties. However, materials science and technology increasingly require analytical probes at the nanoscale, so the spatial resolution of STXM (practical instruments ~30 nm, state-of-art ~8 nm [21]) is a significant limitation.

Over the past decade scanning coherent diffraction imaging, now known as ptychography, has emerged as a high resolution X-ray imaging technique [22,23]. It can be readily implemented as an extension to conventional STXM where it provides 3 – 5 times higher spatial resolution than corresponding STXM images measured at full focus using the same zone plate [24-26]. The spatial resolution of STXM (R) is

* Corresponding author.
E-mail address: aph@mcmaster.ca (A.P. Hitchcock).
[1] Present address: Walker Department of Mechanical Engineering, The University of Texas at Austin, Austin, Texas 78712, USA

https://doi.org/10.1016/j.elspec.2024.147487
Received 9 March 2024; Received in revised form 23 July 2024; Accepted 23 September 2024
Available online 27 September 2024
0368-2048/© 2024 The Author(s). Published by Elsevier B.V. This is an open access article under the CC BY-NC license (http://creativecommons.org/licenses/by-nc/4.0/).

determined by the properties of the Fresnel zone plate used to focus the X-rays, in particular, the diameter (D) and the outer zone width (δr) ($R = D\delta r/\lambda$, where λ is the X-ray wavelength) [1]. Although ptychography performed in a STXM does use a zone plate, in principle the spatial resolution achieved by coherent diffractive imaging (CDI) is not dependent on the properties of lenses. In principle, ptychography can achieve a photon wavelength (λ) limited spatial resolution, $R_{wl} = 0.61\ \lambda/N.A.$, where the numerical aperture (N.A.) is necessarily smaller than 1 [22,27,28]. Thus, in the soft X-ray region (100–2000 eV), spatial resolutions from 7.5 nm to 0.4 nm are potentially achievable. To date the best achieved spatial resolution in soft X-ray ptychography is a full period Rayleigh resolution (1.22 λ/D, where λ is the wavelength and D is the position of the first minimum in the radial distribution of the probe [1]) of 6 nm at 1500 eV [25], which is still 5 times lower than might be achieved in a fully optimized ptychography measurement. There is still room for instrumental and software improvements !

Ptychography uses a high performance X-ray camera to measure transmission diffraction patterns created by a partially or fully coherent X-ray beam impinging on a sample [23,27,28]. Arrays of such diffraction images (DI) sampled in real space with overlap, are reconstructed into real space images and phase maps using an iterative computer algorithm [29–31]. In spectro-ptychography (SP), ptychography images are measured at sequences of X-ray energies spanning one or more X-ray absorption edges. Although the spectral signals in SP are really a refractive index spectroscopy [32], to a first approximation, SP amplitude stacks can be treated in the same way as STXM transmission stacks. The first soft X-ray SP study was performed by Beckers and co-workers [33].

Ptychography [34] can be applied using various fully or partially coherent illumination sources, including visible light [35], electron beam in TEM [36,37], soft [24,25] and hard X-rays [38,39], and laser based extreme ultraviolet (EUV) light [40]. In the last decade, spectro-ptychography performed in soft X-ray STXM instruments has developed significantly (see supplemental information, section SI-1 and Fig. S.1 which summarizes the SP literature to mid-2024). The data presented in SI-1 is excerpted from a bibliography of all soft X-ray microscopy papers [http://unicorn.mcmaster.ca/xrm-biblio/xrm_bib.html]). Of the approximately 2500 papers reporting soft X-ray microscopy published from 1970 to mid-2024, about 4 % involve ptychography. With the use of multiple photon energies, image sequences of ptychographic amplitude and phase images (also called stacks [41]) can be recorded in ways similar to conventional STXM stacks. Thus, chemical mapping using soft X-ray SP [24,26] is now recognized as a higher spatial resolution alternative to chemical mapping using STXM. Soft X-ray SP has been used in many applications, including Li batteries [25,42–45], fuel cells [46], electro-catalysts [47–49], organic photovoltaic materials [50], magnetic bacteria [51], etc.

The purpose of this paper is to report a direct comparison of the results of STXM and SP measurements of the same area of the same electrodeposited Cu particle samples in order to evaluate the relative merits of the two closely related techniques. We have intentionally chosen to study 'real world' samples, rather than artificially optimized "resolution test standards", since this allows a more realistic evaluation of the 'value added' of SP relative to STXM. While the focus of this article is the STXM/SP comparison, the two samples we have investigated are candidate CO_2 reduction electrocatalysts, prepared by slightly different methods. As detailed in the discussion, the differences in morphology and chemical composition can be related to the differences in the sample preparation. The direct comparison documents significant advantages of SP relative to STXM in terms of spatial resolution, spectral chemical mapping, acquisition times, and radiation dose. We conclude that, where feasible, it is better to use SP rather than STXM. The authors hope that this will encourage greater use of SP in the many application areas of soft X-ray microscopy, and also encourage more synchrotron radiation facilities to provide soft X-ray ptychography, especially the 4th generation diffraction-limited storage rings [52] currently operating, under construction or being commissioned. Increased use of SP is expected given (i) the importance of high brightness and coherence to successful ptychography, and (ii) the huge investment in upgrades or new facilities using high brightness fourth generation technology.

2. Experimental

2.1. Sample preparation

2.1.1. Electrodeposition of Cu nanoparticles (samples A & B)

Cu nanoparticles were electrodeposited from a solution of 5 mM $CuSO_4$ and 50 mM KCl onto a thin (15 nm) Au working electrode on a micro-chip device designed for *in situ* flow electrochemical STXM [15] and SP [49]. The electrodeposition solution concentrations and conditions were chosen based on previous reports [47] to target particles in the range of 50−100 nm diameter. The details of the electrodeposition are given elsewhere [15]. Cu nanoparticles prepared in a similar manner were also characterized using scanning electron microscopy (SEM). (supplemental information, Fig. S.2). **Sample A** (measured at the Hermes beamline of Synchrotron Soleil [53]) is in the center region of the electrodeposited Cu samples, where typically the Cu exists as nanoparticles. **Sample B** (measured using the ambient STXM at the spectromicroscopy (SM) beamline at the Canadian Light Source, CLS [54]) is a region at the edge of an electrode of another Cu sample prepared using a slightly different electrodeposition method. In this case, the sample morphology includes both 'chunky' dendrites and both small and large nanoparticles. The more complex morphology of **sample B** as compared to **sample A** is due to the use of a lower potential range for **sample A** (-0.25 to +0.15 V, −10 to +25 μA) than for **sample B** (-0.35 to +0.15 V, −30 to +30 μA; V are relative to Ag/AgCl).

2.2. STXM measurements and data analysis

The STXM measurements for **sample A** were performed using the HERMES beamline at Synchrotron SOLEIL [53]. The STXM measurements for **sample B** were conducted at the spectromicroscopy beamline (SM) 10ID-1 at the Canadian Light Source (CLS, Saskatoon, Canada). Details of the ambient STXM and the SM beamline [54] have been presented elsewhere. Briefly, a monochromatic X-ray beam is focused to a ~40 nm spot by a Fresnel zone plate. The sample is positioned at the focal point of the X-ray beam. Images ware measured by (x,y) raster scanning the sample while recording the transmitted X-ray intensity pixel by pixel in a single photon counting mode using a phosphor/-photomultiplier single X-ray counting detector. STXM images at a single photon energy were measured by scanning the sample while recording the transmitted X-ray intensity pixel by pixel. A STXM stack is a sequence of STXM images collected at various photon energies to provide spatially resolved spectroscopic information about the sample. For **sample A**, a 34 energy Cu $2p_{3/2}$ stack spanning 925–945 eV was used and the same energy values were measured with both STXM and SP. For **sample B**, the sampled energies, spatial range and other experimental conditions were changed between the STXM and SP measurements, as documented in Table 1. These differences are taken into account when making STXM/ptycho comparisons of dose, time, efficiency etc.

All STXM data (and SP derived absorption stacks) were analyzed using aXis2000 software [55]. The analysis consisted of Fourier cross-correlation alignment, conversion from the as-recorded transmission signal to STXM optical density (OD) or SP absorption [4] and photon energy calibration. A fitting procedure based on the singular value decomposition (SVD) matrix method [56] was used to analyze the stacks. The reference spectra used in fitting both the STXM and SP stacks are displayed in Fig. 1. The Cu 2p spectra of Cu metal, Cu_2O and CuO, measured using STXM explicitly for this work, are plotted as points, using an absolute intensity scale, optical density per nm at standard densities (OD1) [4]. Offsets are used for clarity. Superimposed, and on the same absolute OD1 scale are spectra of the same species reported by

Table 1
Summary of parameters used for STXM and spectral ptychography measurements reported in this paper.

Sample	Method	measurement	E (eV)	Calib^{+} (eV)	Spot size (nm)	Slits (μm)	Size (μm)	Sampling (points)	Overlap (%)	Dwell (ms)	reconstruction	Elapsed time (m)	Dose (@) (MGy)
A[&]	STXM	image	933.3		33	20 ×20	2 ×2	60 ×60	-	20	-	1	66
	STXM	Cu 2p stack S221009049	924–946 (34-E)	−5.6	33	20 ×20	2 ×2	60 ×60	-	20	-	90	2000
	ptycho	image	933.3		1000	20 ×20	2 ×2	20 ×20	90	60	AP1000	1	19
	SP	Cu 2p stack S221009046	924–946 (34-E)	−5.6	1000	20 ×20	2 ×2	20 ×20	90	60	AP1000	40	640
B*	STXM	Cu 2p stack A230804005	924–949 (92-E)	−0.33	40	7 ×7	8 ×12	200 ×300	-	2	-	300	160
	SP	Cu 2p stack A230803086	924–949 (58-E)	−0.33	2500	16 ×16	6 ×6	12 ×12	80	310	800	45	750^

+ energy needed to add in order to match the peak of CuO to that of the calibrated CuO reference spectrum (930.54 ±0.05 eV)
& Electrodeposition: −0.25 to +0.15 V, −10 to +25 μA for **sample A**.
* Electrodeposition: −0.35 to +0.15 V, −30 to +30 μA for **sample B** (V are relative to Ag/AgCl).
@ evaluated from dose per pixel, taking into account overlap used. Similar results are obtained if the dose is estimated from the total energy delivered to the whole imaged area over the total time for the measurement.
The beam was on the sample for the total time of the measurements (no shuttering).
^ Note that for the SP measurement at CLS, if the same sized slits as used for STXM were used, the dose would be 1/5th or only 120 MGy.

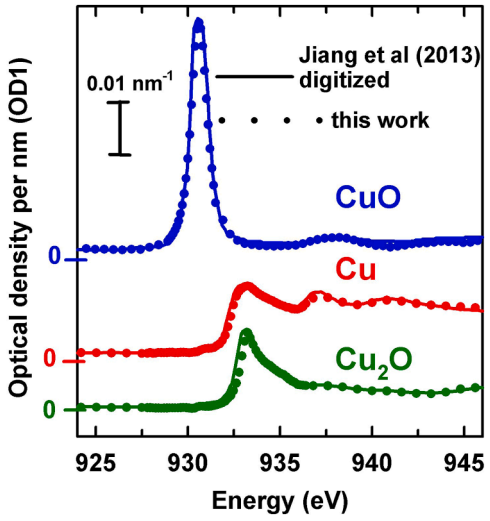

Fig. 1. Cu 2p spectra of Cu metal, cuprous oxide (Cu_2O) and cupric oxide (CuO) plotted on absolute OD1 intensity scale. The dots are experimental data, which were measured at Bessy-II (Cu_2O, CuO) and CLS (Cu). The solid lines are the corresponding spectra digitized from Jiang et al [57]. Offsets, used for clarity, are indicated by the zero intensity indicators.

Jiang et al [57]. There is excellent agreement in spectral shape and feature energies.

The result of fitting a STXM or SP stack to suitable reference spectra is a set of component maps (spatial distributions), one for each component, along with a map of a constant (corresponding to the Au electrode) and the residual of the fit, averaged over all energies of the stack [4]. When reference spectra on OD1 intensity scales (as in Fig. 1) are used in a fit, the gray scales of the derived component maps are an estimate of the average thickness in nm at each pixel measured [4]. In order to verify the chemical mapping and quality of fits, the Cu 2p X-ray absorption spectra (XAS) of selected areas (many pixels, which are not necessarily contiguous, but with similar Cu L_3 spectra) were extracted from the STXM stacks. An example of the fit analysis in the spectral domain is presented in SI-3, Fig. S.3.

2.3. Spectro-ptychographic measurements

In this work a back-illuminated Dhyana-92 or Dhyana-95 camera (Tucsen Inc., China https://www.tucsen.com/) with a coated scientific complementary-metal-oxide-semiconductor (sCMOS) sensor [58] was used to record the diffraction images. The version used for this work was capable of transferring a full 1024 × 1024 (1 Mpixel) 16-bit image in less than 100 ms (current versions have 2048×2048 pixels, and a transfer rate of 48 12-bit images/sec). The well depth is 16-bit and the average background is 70.7±0.3 counts/pixel/60 ms), most of which is from a background associated with the visible light interferometer laser used in the STXM [59]. The background signal is stable over the time to measure an SP stack, but does vary from pixel to pixel so 10 images are measured with the X-ray beam shuttered and the average of those images is subtracted from each DI of a measured ptychography image. The version with the coated sensor (Gpixel GSENSE400BSI) has high quantum efficiency down to 500 eV, while the version without a sensor coating (Gpixel GSENSE400BSIGP) has high sensitivity down to the visible range – see Fig. S.1 of the supplemental information of reference [60]).

In the implementation at the CLS ambient STXM the glass cover of the sensor of the as-received Dhyana-95V2 sCMOS camera was removed, and the camera was mounted on an x,y,z stepper motor stage on which the conventional phosphor-photomultiplier detector was also mounted (see Fig. S.4). The water cooling lines to the integral Peltier cooler are permanently mounted in the ambient STXM. The data signal is transmitted through the STXM vacuum tank using a double sided USB3.0 (male-male) feedthrough. The x-axis (horizontal) range of the detector stage is 100 mm, allowing either the STXM or the ptychography detector to be positioned and centered on the X-ray axis of the monochromated X-ray beam.

At the STXM on the Hermes beamline at synchrotron SOLEIL the Dhyana-92V1 sCMOS camera (the first version, supplied without water cooling) has been heavily modified. A Peltier chiller with water cooling was added and the read-out electronics were rebuilt such that only the first stage of readout is inside the STXM tank with all other parts of the readout electronics outside the STXM tank (see Fig. S.5). At the time of these measurements (Oct 2022), it was necessary to remove the conventional phosphor-photomultiplier detector and physically mount and center the Dhyana camera. This is somewhat time consuming (~2 h) and a task needing considerable care and expertize. So, although most functions can be performed in ptychography mode (albeit, somewhat

awkwardly), typically microscope and beamline tuning, focusing, region of interest selection and spectroscopic checks such as energy calibration and thickness determination are performed prior to changing from STXM to SP mode. The SP acquisition software at the Hermes STXM (custom written python code) can be used in a STXM-like mode where, at each position in the image, it only records an integral of the central area which includes all of the unscattered light – and thus the equivalent to the STXM signal. This mode was used for the STXM results presented in Fig. 2 & 3. In addition, when a very large defocus is used, the camera image becomes a type of projection, full field imaging microscope which can be very useful for navigation. We note that recently the detector set-up at the Hermes STXM has been modified so that both the ptychography camera and the phosphor-photomultiplier detector co-exist in the STXM tank and one can change from STXM to SP mode without opening the STXM tank.

2.4. Ptycho acquisition and data analysis

2.4.1. Ptycho acquisition

Ptychography measured using the smallest spot size achievable, with a zone plate or other X-ray focusing, and spot overlaps of 20–40 % has been used in many previous X-ray spectro-ptychography (SP) studies [25,46,61]. However the key to the many advantages provided by SP relative to conventional STXM described in this article is the use of an intentionally defocused X-ray spot size. Ptychographic imaging with a defocused electron spot size has been adopted in the scanning transmission electron microscopy (STEM) community to reduce radiation damage while at the same time achieving phase imaging with a spatial resolution beyond the diffraction limit [36]. Use of defocused spot sizes in soft X-ray transmission microscopy was first reported by Xu et al [62]. Due to the advantages of (i) fewer numbers of DI images per ptycho image, and (ii) reduced radiation damage/ DI, defocused spot sizes are being used increasingly [42,60]. Procedures to optimize parameters such as spot overlap [63] and detector distance from the sample [64] are published elsewhere.

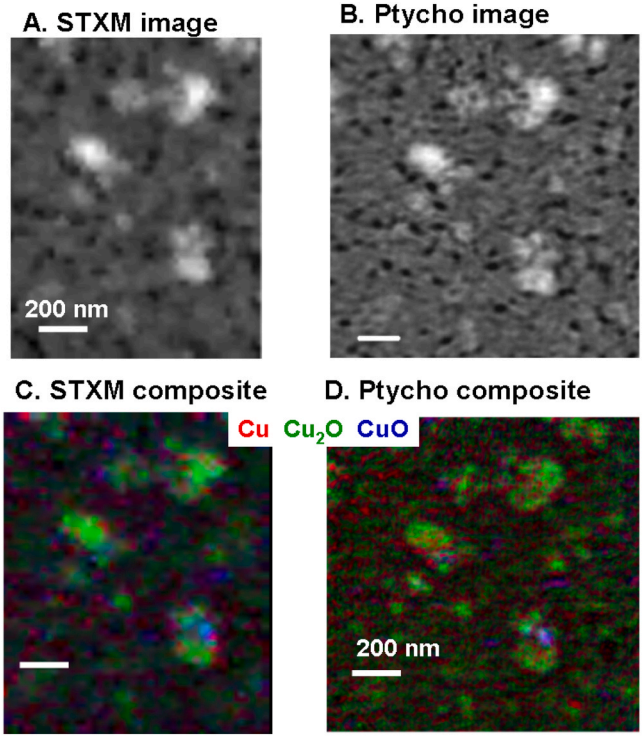

Fig. 2. Comparison of imaging and chemical mapping by STXM and SP of sample A. (a) STXM transmission image at 933.3 eV. (b) ptychography amplitude image at 933.3 eV. Color coded composite of Cu (red), Cu_2O (green), and CuO (blue) component maps, derived from (c) the fit of a 34 energies Cu L_3 STXM stack (~90 m) and (d) the fit of an SP (Ptycho) 34 energies Cu L_3 stack (30 m).

In this work the position of the sample (Soleil) or the zone plate (CLS) was intentionally displaced from the full focus position in order to have an annular spot (from the projection of the zone plate zones) with an outer diameter of 1 μm at Soleil and 2.5 μm at CLS. When defocused spot sizes are used it is important to choose a step size that will achieve a high degree of overlap of adjacent spots, typically 80 – 90 %. An experimental demonstration of the effect of sampling overlap for a 1 μm spot size on the quality of the ptychographic reconstruction was presented earlier [60]. For **sample A** (Soleil), the exposure time for each diffraction image (DI) was 60 ms for the 1 μm ptychography stack measurement, which was the minimum time required to integrate for 50 ms dwell and transfer the image to the acquisition computer. For **sample B** (CLS), the exposure time for each diffraction image (DI) was 310 ms for the 2.5 μm defocused ptychography stack measurement,. This longer exposure was selected to improve the quality of individual DI, relative to the fastest possible acquisition (~60 ms/DI at the CLS installation). The emittance of CLS (18 nm.rad) is much larger than that of Soleil (4 nm. rad), and thus the coherent fraction is lower.

2.4.2. Reconstruction using PYNX

The ptychography data for **sample A** was reconstructed using the open-source Python tools for Nano-structures Xtallography (PyNX) software [65], developed at the European Synchrotron Radiation Facility. 200 iterations of the Alternate Projection (AP) algorithm with a single probe function (AP**200) was used for the initial analysis. At a later time, the data was re-processed using a 2 stage processing in which 3 probe functions and AP**1000 iterations was followed by a 1 probe, AP**50 iteration reconstruction. The more complex reconstruction typically reduces the extent of raster grid artifact [66,67], and improves the spatial resolution (see SI-5, Fig. S-6). Two different computer set-ups were used to process the ptycho data at the Hermes beamline – the first one with fewer GPUs but a faster CPU which was used for checking and parameter optimization on a single image; while the second one featured a slower CPU but many more GPUs, which was used for unsupervised processing of stacks. Typical processing times with the Soleil computer network and processors are 5 min/image for AP**200 and 20–30 minutes/image for AP**1000.

2.4.3. Reconstruction using PyPIE

The ptychographic data sets for **sample B** were reconstructed using the PyPIE software package, developed by the CLS SM beamline team [42,68]. PyPIE is a CPU-based python program using the extended Ptychographical Iterative Engine (ePIE) algorithm [34,35]. PyPIE and the computational platform at CLS is considerably slower that the PYNX setup at Soleil. However automated procedures to process a stack by dedicating individual CPUs of a 40-CPU computer are used to facilitate the data processing. Typically using PyPIE to process a ptychography data set for one image consisting of 144 DI would take ~50 m. Since multiple processors (1 / energy) are used when processing stacks, the time to process an <80 energy stack is only twice the time to process a single image.

3. RESULTS

3.1. Comparing STXM and SP of Cu nanoparticles at Soleil (sample A)

Fig. 2 compares STXM (Fig. 2**a**) and ptychography (Fig. 2**b**) images at 933.3 eV, the peak energy of Cu L_3 absorption of Cu metal and Cu_2O) of deposited Cu particles (**sample A**). The detailed parameters for each measurement are listed in Table 1. The time for a STXM image acquisition (~3 min) is 3 times longer than the corresponding ptychography image acquisition (~ 1 min). Despite a shorter measurement time, the resulting ptychography image has better spatial resolution and

statistical precision which allows better visualization of fine, weakly absorbing particles. The spatial resolution in the SP image is ~3x better than that of the STXM image, as demonstrated by comparisons of line profiles over the same position on the sample (see SI-6, Fig. S.7). The 34 energy STXM stack took 90 m to record while the corresponding SP stack took only 30 m. The radiation doses for the STXM and SP stacks were calculated using standard methods described elsewhere [69,70]. Details and results are presented in section SI-8, Table S-2, while the total dose for each measurement is listed in Table 1. The estimated dose imparted to record the SP stack is 640 MGy while the estimated dose for the STXM stack is 2000 MGy.

The color coded composites of the component maps of Cu, Cu_2O and CuO, derived by stack fitting the STXM and SP stacks are presented in Figs. 2**c** and 2**d**. The individual, quantitative component maps are presented in Fig. 3. The color-coded chemical mapping using SP has improved spatial resolution relative to that derived from STXM (see Figs. 2**c,** 2**d** and section SI-6, Fig S.7, for detailed spatial resolution evaluation). The quantitative spatial distributions of Cu, Cu_2O and CuO in SP mapping are similar to those derived from STXM, but with much higher spatial resolution, such that small Cu(I) nanoparticles ~50 nm can be observed. (compare Fig. 2**c** and **d**) Note that a more sophisticated ptychographic reconstruction was needed to properly visualize the nanoparticles (compare Fig. S.6c and S.6d). Our measurements on **sample A** indicate that SP with a 1 μm spot size imparts about 3 times lower dose than STXM, performs the acquisition in a significantly shorter time (~1/3rd), provides better statistical precision, and much better spatial resolution.

Fig. 3 presents the component maps from the fitting analysis of the Cu $2p_{3/2}$ STXM and SP stacks. Fig. 3 **a-c** show the quantitative maps of the Cu, Cu_2O and CuO distributions derived from the STXM stack, while Fig. 3 **d-f** presents the corresponding maps from SP. The results from both analyses are in good agreement. They indicate that the particles are mainly Cu_2O with small amounts of Cu metal and CuO. There are also a few localized CuO particles. The SP composite maps are similar to those of STXM, both in terms of spatial distributions and quantitative thickness estimates. However, in the Cu_2O component map measured by SP small Cu nanoparticles with size of ~ 50 nm and thickness ~10 nm can be clearly observed, while these are observed much less clearly in the STXM maps.

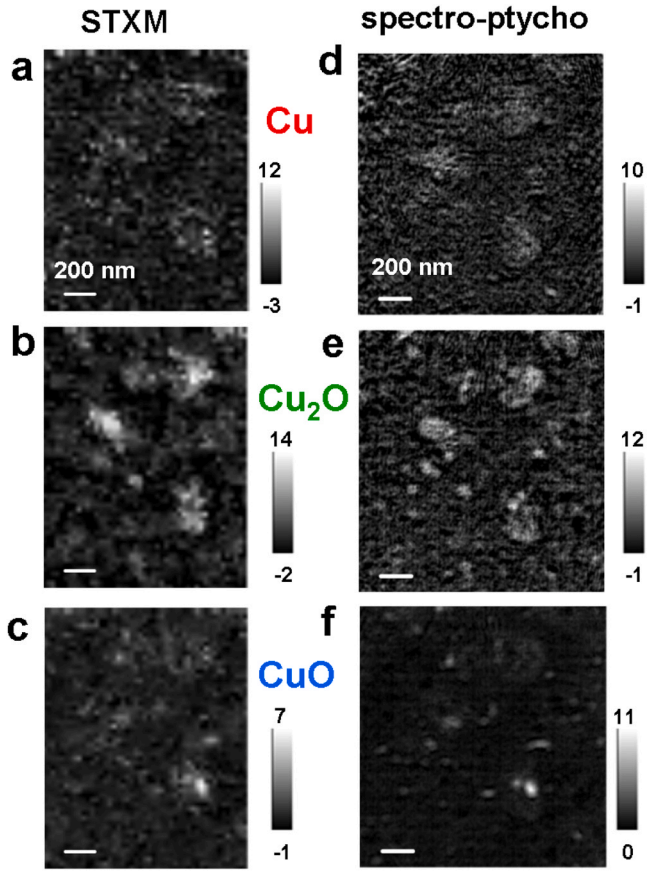

Fig. 3. Comparison of component maps derived from the STXM and SP stack fit of sample A. Component maps from STXM stack fit for (a) Cu, (b) Cu_2O and (c) CuO. Component maps from SP stack fit for (d) Cu, (e) Cu_2O and (f) CuO. The intensity scales show the thickness in nm.

To confirm the SP mapping result, the spectra of Cu-rich, Cu_2O-rich and CuO-rich regions were extracted by threshold masking the component maps and analyzed to verify the quantitative composition of each region (Fig. S-3)**.** The results of the spectral fit results are consistent with the mapping fits (Fig. 3), confirming that Cu, Cu_2O and CuO are the dominant species in the corresponding regions. Results from the spectral-domain analysis for each component and for both STXM and SP measurements are summarized in Table 2.

3.2. *Comparing STXM and SP of Cu nanoparticles at CLS (sample B)*

Fig. 4 compares color-coded composites of the Cu, Cu_2O and CuO chemical maps derived from STXM (Fig. 4**a**) and SP (Fig. 4**b**) stacks of the electro-deposited Cu in **sample B**. The small size of the Cu nanoparticles and better quality of chemical mapping show the advantages of the higher spatial resolution of SP (~20 nm), compared with STXM (~60 nm). Fig. 5 shows the component maps from the STXM (Fig. 5 **a-c**) and SP stacks (Fig. 5 **d-e**). The SP chemical maps show much finer detail than the STXM maps, resulting in higher chemical sensitivity. This is shown more clearly when one examines small areas of Fig. 5 where there are large changes in the chemical composition over a short distance - see Fig. S8,Section SI-9**.** In terms of chemical mapping and chemical sensitivity, SP clearly outperforms STXM. In addition, the results demonstrate the faster acquisition and lower radiation damage when the measurements are performed by SP than by STXM. The STXM stack took ~ 300 min and delivered a radiation dose of 160 MGy. Although it imparted a larger dose (750 MGy), the SP stack took only 45 min.

We note that there are regular diagonal stripes over ~1/3rd of Fig. 4 a and Fig. 5**b** (above the dendritic structures at the bottom). This moiré pattern is an artifact of the CLS aSTXM system which is caused by beating between the frequency of the raster scan image measurement and a ~1 Hz oscillation of the incident X-ray intensity. Despite much effort to identify the source of the intermittent intensity oscillation, it has not been able to eliminate it and thus such stripes can appear when the incident flux oscillation occurs. Note that there is no trace of the modulation in the SP counterpart (Fig. 4**b** and Fig. 5**e**), which supports our interpretation and points to an additional advantage of SP over

Table 2
Compositions of Cu, Cu_2O and CuO rich regions[a] of **sample A** from STXM and SP[b].

Regions	Volume percentage (%)					
	Cu		Cu_2O		CuO	
	SP	STXM	SP	STXM	SP	STXM
Cu rich	**46 ± 5**	**49 ± 5**	35 ± 4	26 ± 3	19 ± 3	15 ± 3
Cu2O rich	14 ± 3	9 ± 3	**75 ± 8**	**79 ± 8**	11 ± 3	12 ± 3
CuO rich	21 ± 3	7 ± 3	23 ± 3	45 ± 3	**56 ± 6**	**48 ± 5**

a. "Same areas" selected
b. The uncertainties combine statistical variation (±3 %) and estimated systematic uncertainties. The latter was estimated by examining how the derived composition varied with slight but reasonable changes in the analysis procedure, such as (i) changing the set of pixels from which the Cu-rich, Cu2O-rich and CuO-rich were extracted and (ii) modifying the composition until a significant degradation of the match of the fit and the experimental spectrum could be observed (see Fig. S.3).

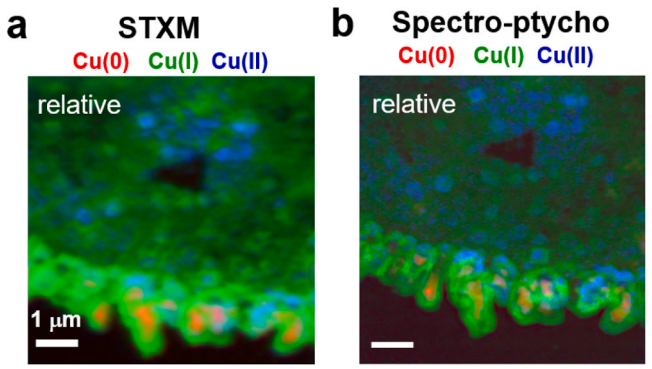

Fig. 4. Comparison of chemical mapping by STXM and SP of sample B. Color coded composite of Cu (red), Cu_2O (green), and CuO (blue) component maps, derived from (c) the fit of a 92 energy Cu L_3 STXM stack (~6 hrs) and (d) the fit of a 57 energy SP (spectro-ptychography) Cu L_3 stack (~45 mins).

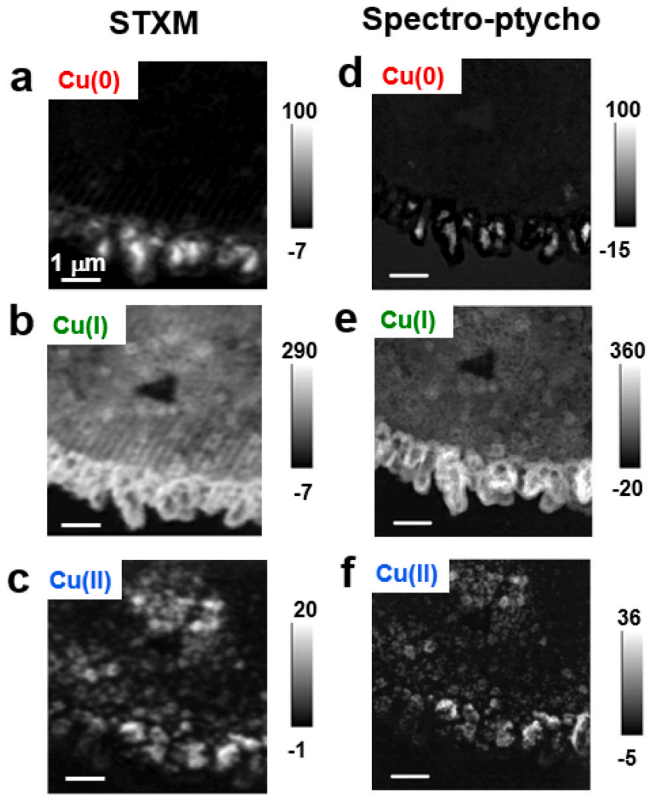

Fig. 5. Comparison of component maps of sample B derived from stack fits of the STXM (92 E) and SP (57 E). Component maps from STXM stack fit for (a) Cu, (b) Cu_2O and (c) CuO. Component maps from SP stack fit for (d) Cu, (e) Cu_2O, and (f) CuO. The intensity scales show the thickness in nm.

STXM in cases where there are intensity modulations leading to periodic artifacts.

4. Discussion

4.1. SP vs. STXM: advantage SP

In this section we note the key reasons for using SP rather than conventional STXM. First is the **quality of the result**. The ptychography images and component maps for **sample A** measured at Synchrotron Soleil at the Cu L-edge (Figs. 2 and 3) and those for **sample B** measured at CLS (Figs. 4 and 5) show better spatial resolution (~12 nm in SP, versus ~55 nm for STXM at Soleil – see Fig S.7); better chemical sensitivity than STXM, and better statistical precision due to the much smaller pixel sizes in the reconstruction (5 or 10 nm in SP, versus 30–40 nm in STXM). The improved chemical sensitivity is in part due to the improved spatial resolution, but also due to the finer spatial sampling (e.g., 5 nm in SP versus 20 nm for STXM for **sample A**) and better statistics of the ptychography.

In addition to better quality results, the SP stacks were measured in a **shorter time** than the corresponding STXM stacks. For **sample A** the 34 energy Cu L_3 SP stack took 40 m, versus 90 m for the same 34 energies measured by STXM; for **sample B**, the STXM and ptychography scans measured different sized areas and number of images. When corrected to the same number of energies and same area measured, the SP acquisition took 45 min versus 85 min for the equivalent Cu L_3 STXM stack. In general, defocused SP measurements take less time to measure than STXM measurements over the same area, thus providing more information within a fixed elapsed time. If the STXM stack was measured with the same spatial sampling as achieved by ptychography (5 nm) the elapsed time and thus dose would be increased by a factor of 35.

Perhaps more crucially, defocus ptychography can deliver significantly **lower radiation dose** than STXM. The calculated doses (see SI-8) indicate that for **sample A** the SP dose was about 1/3rd of the STXM dose. For **sample B**, although the dose delivered by SP was higher (750 MGy) than the STXM dose (160 MGy), this was because a long dwell (310 ms /DI) was used. If the dwell used for **sample B** was the same as used for **sample A** (60 ms), the SP dose for **sample B** would be smaller (120 MGy) than the STXM dose (160 MGy). Since the same camera was used for the CLS and Soleil measurements, if the source brightness, beamline efficiency etc. were the same one should be able to use the same acquisition time / DI.

The reduced dose for ptychography measurements may surprise some readers. In early soft X-ray ptychography measurements [25] the dose for SP was much larger than for the corresponding STXM since a fully focused beam spot was used and the slits were opened to increase the incident flux by 1–2 orders of magnitude (~10^7 ph/s for STXM to ~10^9 ph/s for SP) in order to achieve improved statistics at higher q (regions of the diffraction images far from the center). With use of defocused beam spots, as in this work, the dose is significantly reduced. In addition, in earlier work, due to use of slow read-out CCD cameras (1 s/image, but only 20 – 100 ms acquisition [46,51] and keeping the beam shutter open through the whole measurement time meant a very high dose. Acquisition options which can reduce dose while achieving similar quality results are very important in soft X-ray microscopy since radiation damage is a limiting factor in many soft x-ray spectro-microscopy studies [71,72]. Closing fast shutters except during the exposure time used to record each DI should be implemented.

These results, and many other examples (see Table S-1), clearly show ptychography routinely achieves significantly better spatial resolution than STXM. We do not claim that these results are the best SP can do in terms of spatial resolution. We also note that these samples are not optimal for a precise spatial resolution determination, as discussed in section SI-6. The best reported spatial resolution (full-period) in soft X-ray SP is 6 nm [25]. . Even if the 'best ptychography' is not achieved, a resolution improvement is invariably observed. Given the other advantages – shorter time, lower dose, better statistical precision – it would seem obvious that SP should be the preferred mode for spectral-imaging rather than STXM.

4.2. SP vs. STXM: advantage STXM

Let us now consider the ways where SP and STXM differ, in order to (i) identify factors that presently discourage researchers from using SP, and (ii) identify ways whereby these barriers might be lowered, thus enabling more routine use of SP.

4.2.1. Ease of use

While SP data sets can be acquired with significantly lower amounts of beam time than STXM, STXM provides interpretable results immediately, whereas there is usually a delay of many hours or even days to get real-space images from SP due to the reconstruction time needed. Thus, it is generally not practical to do initial navigation, focusing, and quality optimization using SP from the very start. Of course, the solution to this is to have rapid and reliable switching between conventional STXM and SP modes. This is the case at ALS [73], and CLS, and was recently implemented at Soleil. Significant progress has been made recently at the COSMIC beamline at ALS, such that it is now possible to perform ptychographic reconstructions in parallel with acquisition so that SP measurements can be monitored in quasi real-time.

4.2.2. Ptychographic reconstruction is 'black-box'

Although the authors have used SP for many scientific studies (see references in SI-1), only a few of them have been directly involved in writing codes for ptychographic analysis. This will be the situation for most future users of SP. Our experience is that, while the expertize and guidance of the ptychography reconstruction experts is very much appreciated, the ability to be able to explore different reconstruction methods and parameter choices, is highly desireable to build user confidence in the robustness of the ptychography reconstruction. Unfortunately, it is often the case that the reconstruction is done by someone else, and that there is insufficient time or restricted access to the computational resources set up for reconstruction to really explore optimization of the many parameters involved. Frankly, the process is most frequently experienced as a painful & 'puzzling' 'black-box' procedure. As the hardware gets more powerful, and the software and user interface more straightforward to use, this situation should improve. Standardization and assistance with implementing the ptychographic reconstruction packages on high-performance computing platforms would be a very helpful development.

4.2.3. SP amplitude signals differ from STXM transmission signals

In fact, SP is really a **refractive index spectroscopy**, not an X-ray absorption spectroscopy. Chemical information is actually contained in both the amplitude and phase signals. So far, this deeper understanding has not been explored to any great extent, although Farmand et al [32]. have shown that SP amplitude and phase signals can be processed simultaneously to considerable advantage. So far, some progress has been made with heuristic analysis of chemical signatures in the phase results by generating reference phase spectra, guided by the amplitude analysis [26,46,48], but it is very unlikely this approach will be robust, due to the strong impact of rapid structural changes on the phase signals [32]. It is also the case that samples with strong chemical signals but low scattering capability (e.g., single atom catalyst regions in Ni-MC catalysts [48]) are detected more easily in STXM than SP.

4.3. Progress to making SP more accessible and better integrated with STXM

Although soft X-ray SP shows many advantages relative to corresponding STXM, there are still many challenges which need to be overcome to make the technique more routine and more widely available. These challenges include:

* difficult to apply over large areas (>10 μm) due to computational resource limitations at most facilities. While this really limits the ability to perform coarse navigation by SP, in fact a small FoV is typically needed to show the detail that the high resolution of SP can provide. In addition, it is possible to tile SP measurements of adjacent regions if high spatial resolution over large areas is required.

* often a 'black box' reconstruction may limit quality of results (see SI-5, Fig. S.6 for an example where a more sophisticated ptychographic reconstruction resulted in vastly improved results).

* Typically, the first step in many 'black box' recipes is binning. However, for strongly scattering samples, this can reduce spatial resolution. Similarly, it is common to restrict the q-range accessed either by truncating the DI or moving the detector farther downstream of the sample. Again, this can lead to a lower spatial resolution than could be achieved without restricting the q-range.

* Because the set-up and data processing for SP is more complex than conventional STXM it is difficult to use SP when other complexities of the experiment, such as *in situ* or operando devices, have to be achieved at the same time. We note that Bozzini and coworkers have pioneered the combination of SP and *in situ/operando* studies of electrochemical systems [74–76]. Our group has recently reported an *in situ* flow liquid electrochemical SP study of copper CO_2 reduction electro-catalysts[49]. Given the challenges of both SP and *in situ* liquid electrochemistry individually, success of these types of complex experiments point to the steadily improving reliability and maturity of SP.

Some of these challenges have been relieved to a degree due to recent breakthroughs in soft X-ray SP instrumentation and techniques. These include:

- substantial reduction of the measurement time due to adoption of sCMOS rather than CCD cameras. sCMOS cameras can typically transfer megapixel images in 10's of ms, as opposed to a typical ~1 s image transfer time for CCDs (exceptions exist);
- improved automation and speed of ptychographic reconstruction [39,62];
- extension of SP to lower photon energies, such as measurements below 500 eV [60,77];
- application of SP to *in situ* flow electrochemical studies of electrocatalysts [49,74–76].
- high-throughput SP for complex studies, such as determining the mechanism of the heterogeneous intercalation / de-intercalation reaction involved in $LiFePO_4$ based lithium batteries [43,44]
- Recently Fe L-edge SP was combined with C 1s STXM results of an organic-organic interface in order to improve the combined spatial resolution [78].

4.4. SP and STXM: lowering the barriers

We note that Du et al [79]. have recently presented an alternate perspective on the benefits of using SP as a means to provide chemical imaging with minimal radiation damage. They showed that the extent of radiation damage is independent of the method that is used to measure ptychography, including measuring at the Fourier (near-field) or Fraunhofer (far-field) limits, use of focus or defocus spot, or considering either phase or amplitude. They point out that the radiation dose only depends on the fluence delivered to the sample and the X-ray absorption properties of the sample. In the abstract of that paper it is claimed: … *(if the experiment and image reconstruction are done properly) the sample can be near or far; wherever you are, photon fluence on the specimen sets one limit to spatial resolution.*"

If a lower degree of overlap can be used, the dose for SP would be greatly reduced since dose increases with the square of the overlap. Witwer and Modregger [80] have recently shown that the spatial overlap needed for reliable reconstruction can be significantly reduced if a real space image is used as the initial guess for the object. Although most reconstruction codes do not do this, for SP systems that use STXM as the platform, it is very straight forward to record a suitable STXM image before (or after) SP and use it as the initial guess for the object.

Machine learning methods (ML, "AI") to ptychographic reconstruction are starting to appear [81,82]. While making the data processing even more of a 'black box', ML methods will take advantage of prior successes in reconstruction, possibly leading to more robust ptychographic reconstruction. Chang et al [83]. recently proposed and developed code where there is simultaneous use of the information from all energies of an SP stack. This involved solving the blind X-ray spectro-ptychography problem, based on coupling the diffraction data

from each photon energy and iteratively retrieving the chemical map of the sample. Liu et al [84]. have presented a periodic-artifact suppressing algorithm (PASA) reconstruction which seems to remove raster-scan artifacts without necessitating alternative acquisition methods such as Fermi spiral scanning [85]. Use of multi-slice methods (i.e. more than one probe or object function displaced along the propagation axis) [86] can be very helpful to deal with samples where the thickness is greater than the depth of focus or where there are variations of chemistry or morphology in the propagation direction.

4.5. On the origin of differences between sample A and sample B

The two samples we have investigated are candidate CO_2 reduction electrocatalysts, prepared by slightly different methods. The significant differences in morphology and chemical composition can be related to the differences in the sample preparation. **Sample A** is an excellent example of the type of mixed Cu(0)/Cu(1) nanoparticles that are being extensively investigated by many groups as candidate electro-catalysts for CO_2 reduction to C2+ products [15,47]. **Sample B**, made by a similar electrodeposition methodology, has a different structure with more Cu material and a much larger, complex set of dendritic growth at the edge of the working electrode (WE).The dendritic growth seems to be linked to use of different limits in the cyclic-voltammetry deposition protocol for Sample B (see Section 2.1.1), Understanding the control factors for determining morphology and chemical composition is an important and integral part of optimization of this system.

5. Summary

This paper has reported direct comparisons of STXM and SP in order to evaluate the relative merits of the two closely related techniques. The significant advantages of defocused SP relative to STXM were documented. Relative to conventional STXM, SP can do all that STXM can do (and more), and do it faster, with better spatial resolution, better precision, lower dose (& thus less damage) and provide similar chemical information. Based on steady improvement in cameras, acquisition strategy (e.g., Fermi spiral scans, which eliminate raster scan artifacts [80,84,85]), data management, processing computers and clusters (especially multi-CPU and multi-GPU systems), and improved algorithms, we expect that SP will ultimately come to dominate over conventional STXM, especially when the highest possible performance and lower radiation dose are needed.

We conclude that, where feasible, even today, it is better to use SP rather than STXM where appropriate (scan areas <10 μm; strong scatterers). Improved support of general users to acquire and process ptycho data, both on-site, and remotely, and to have the ability to optimize the reconstruction and subsequent processing are needed if SP is to achieve its potential as a premier method of analytical soft X-ray microscopy. The authors hope that this article will encourage greater use of SP in the many application areas of soft X-ray microscopy, and also encourage more synchrotron radiation facilities to provide soft X-ray ptychography, especially the 4th generation facilities (diffraction limited storage rings [1]) that are currently operational, under construction or commissioning [52]). Indeed, increased use of SP is expected given (i) the importance of high brightness and coherence to successful ptychography, and (ii) the huge investment in upgrades or new facilities using high brightness fourth generation technology.

CRediT authorship contribution statement

Jian Wang: Writing – review & editing, Supervision, Software, Project administration, Investigation, Funding acquisition, Formal analysis, Conceptualization. **Stefan Stanescu:** Software, Investigation. **Tianxiao Sun:** Software, Methodology, Investigation. **Haytham Eraky:** Writing – review & editing, Investigation. **Drew Higgins:** Writing – review & editing, Resources, Funding acquisition. **Adam Hitchcock:** Writing – original draft, Resources, Project administration, Investigation, Formal analysis, Data curation, Conceptualization. **Chunyang Zhang:** Writing – review & editing, Investigation. **Sufal Swaraj:** Investigation. **Rachid Belkhou:** Software, Resources, Methodology, Funding acquisition. **Nicolas Mille:** Software, Methodology, Investigation, Formal analysis.

Declaration of Competing Interest

The authors declare that they have no known competing financial interests or personal relationships that could have appeared to influence the work reported in this paper.

Data availability

Data will be made available on request.

Acknowledgments

We acknowledge synchrotron SOLEIL for the provision of beamtime (proposal No. 20220343). We thank the staff of the CLS Spectromicroscopy beamline– Yingshen Lu, Jay Dynes – for their assistance. We thank Dr. Vincent Favre-Nicolin for providing the PYNX software used for processing Soleil ptychography datasets. Cu 2p spectra of Cu_2O and CuO were measured at the Mystiic beamline at Bessy-II, which is supported by the energy-materials *in situ* Lab (EMiL) of the Fritz-Haber Institute at Bessy-II. We thank the Helmholtz-Zentrum Berlin für Materialien und Energie for the allocation of beamtime. Research performed at the Canadian Light Source supported by the Canadian Foundation for Innovation. This research was supported by the Natural Sciences and Engineering Research Council (NSERC) Discovery Grant program, the National Research Council of Canada (NRC) Materials for Clean Fuels Challenge program, and by TotalEnergies and a related NSERC Alliance grant

Appendix A. Supporting information

Supplementary data associated with this article can be found in the online version at doi:10.1016/j.elspec.2024.147487.

References

[1] C.J. Jacobsen, X-Ray Microscopy, Cambridge University Press, 2019.
[2] H. Ade, A.P. Hitchcock, NEXAFS microscopy and resonant scattering: Composition and orientation probed in real and reciprocal space, Polymer 49 (2008) 643–675.
[3] Tae Hyun Yoon, Applications of soft X-ray spectromicroscopy in material and environmental sciences, Appl. Spectrosc. Rev. 44 (2009) 91–122.
[4] A.P. Hitchcock, Soft X-ray Imaging and Spectromicroscopy Chapter 22 in Volume II (Methods) of the Handbook on Nanoscopy, eds. Gustaaf Van Tendeloo, Dirk Van Dyck and Stephen J. Pennycook (Wiley, 2012) 745-79.
[5] J. Cosmidis, K. Benzerara, Soft X-ray scanning transmission spectromicroscopy, Biominer. Sourceb.: Charact. Biominer. Biomim. Mater. (2014) 115–133.
[6] Stöhr, J., NEXAFS spectroscopy, Springer Series in Surface Science, Vol 25 (Springer, Berlin, 1992).
[7] A.E. Goode, A.E. Porter, M.P. Ryan, D.W. McComb, Correlative electron and X-ray microscopy: probing chemistry and bonding with high spatial resolution, Nanoscale 7 (2015) 1534–1548.
[8] J. Wang, G.A. Botton, M.M. West, A.P. Hitchcock, Quantitative evaluation of radiation damage to polyethylene terephthalate by soft X-rays and high-energy electrons, J. Phys. Chem. B 113 (2009) 1869–1876.
[9] E. Najafi, A.P. Hitchcock, D. Rossouw, G. Botton, Mapping defects in a carbon nanotube by momentum transfer dependent electron energy loss spectromicroscopy, Ultramicroscopy 113 (2012) 158–164.
[10] H. Ali, T. Warnatz, L. Xie, B. Hjorvasson, K. Leifer, Quantitative EMCD by use of a double aperture for simultaneous acquisition of EELS, Ultramicroscopy 196 (2019) 192–196.
[11] L.G.A. Melo, A.P. Hitchcock, Electron beam damage of perfluorosulfonic acid studied by soft X-ray spectromicroscopy, Micron 121 (2019) 8–20.
[12] I. Martens, L.G. Melo, M.M. West, D.P. Wilkinson, D. Bizzotto, A.P. Hitchcock, Imaging reactivity of the Pt–ionomer interface in fuel-cell catalyst layers, ACS Catal. 10 (2020) 8285–8292.
[13] C. Zhang, L. Shahcheraghi, F. Ismail, H. Eraky, H. Yuan, A.P. Hitchcock, D. Higgins, Chemical structure and distribution in nickel–nitrogen–carbon catalysts for CO2

electroreduction identified by scanning transmission X-ray microscopy, ACS Catal. 12 (2022) 8746–8760.
[14] W. Yang, H. Eraky, C. Zhang, A.P. Hitchcock, I. Zhitomirsky, Scanning transmission X-ray microscopy studies of electrochemical activation and capacitive behavior of Mn_3O_4 supercapacitor electrodes, J. Mater. Chem. A 10 (2022) 18267–18277.
[15] C. Zhang, H. Eraky, S. Tan, A. Hitchcock, D. Higgins, In-situ studies of copper-based CO2 reduction electrocatalysts by scanning transmission soft X-ray microscopy, ACS Nano 17 (2023) 21337–21348.
[16] J. Kim, D. Lee, C. Nam, J. Chung, B. Koo, N. Kim, J. Lim, Energy material analysis via in-situ/operando scanning transmission x-ray microscopy: a review, J. Electron Spectrosc. Relat. Phenom. 266 (2023) 147337.
[17] Chuntian Cao, Michael F. Toney, Tsun-Kong Sham, Ross Harder, Paul R. Shearing, Xianghui Xiao, Jiajun Wang, Emerging X-ray imaging technologies for energy materials, Mater. Today 34 (2020) 132–147.
[18] Jigang Zhou, Jian Wang, Applications of soft X-ray spectromicroscopy in energy research from materials to batteries, Adv. X-ray Imaging Electrochem. Energy Mater. Devices (2021) 141–178.
[19] Jun Zhong, Hui Zhang, Xuhui Sun, Shuit-Tong Lee, Synchrotron soft X-ray absorption spectroscopy study of carbon and silicon nanostructures for energy applications, Adv. Mater. 26 (46) (2014) 7786–7806.
[20] Jungjin Park, Seong-Jun Kim, Kookhan Kim, Yunseo Jeoun, Seung-Ho Yu, Chunjoong Kim, Yung-Eun Sung, Elton J. Cairns, Understandings about functionalized porous carbon via scanning transmission x-ray microscopy (STXM) for high sulfur utilization in lithium-sulfur batteries, Nano Energy 100 (2022) 107446.
[21] B. Rösner, F. Koch, F. Döring, V.A. Guzenko, M. Meyer, J.L. Ornelas, A. Späth, R. H. Fink, S. Stanescu, S. Swaraj, R. Belkhou, B. Watts, J. Raabe, C. David, 7 nm spatial resolution in soft X-ray microscopy, Microsc. Microanal. 24 (2018) 270–271.
[22] F. Pfeiffer, X-ray ptychography, Nat. Photonics 12 (2018) 9–17.
[23] J. Rodenburg, A. Maiden, Ptychography, Springe Handb. Microsc. (2019) 819–904.
[24] A.P. Hitchcock, Soft X-ray spectromicroscopy and ptychography, J. Electron Spectrosc. Relat. Phenom. 200 (2015) 49–63.
[25] D.A. Shapiro, Y.S. Yu, T. Tyliszczak, J. Cabana, R. Celestre, W. Chao, K. Kaznatcheev, A.D. Kilcoyne, F. Maia, S. Marchesini, Y.S. Meng, Chemical composition mapping with nanometre resolution by soft X-ray microscopy, Nat. Photonics 8 (2014) 765–769.
[26] S.G. Urquhart, X-ray Spectroptychography, ACS Omega 7 (2022) 11521–11529.
[27] Pierre Thibault, Martin Dierolf, Andreas Menzel, Oliver Bunk, Christian David, Franz Pfeiffer, High-resolution scanning X-ray diffraction microscopy, Science 321 (2008) 379–382.
[28] C.G. Schroer, P. Boye, J.M. Feldamp, J. Patommel, A. Schropp, A. Schwab, S. Stephan, M. Burghammer, S. Schöder, C. Riekel, Coherent X-ray diffraction imaging with nano-focused illumination, Phys. Rev. Lett. 101 (2008) 1–4.
[29] J.R. Fienup, Reconstruction of an object from the modulus of its fourier transform, Opt. Lett. 3 (1978) 27–29.
[30] J. Miao, D. Sayre, H.N. Chapman, Phase retrieval from the magnitude of the Fourier transforms of nonperiodic objects, J. Opt. Soc. Am. A 15 (1997) 1662.
[31] J. Miao, P. Charalambous, J. Kirz, D. Sayre, Extending the methodology of X-ray crystallography to allow imaging of micrometre-sized non-crystalline specimens, Nature 400 (1999) 342–344.
[32] M. Farmand, Richard Celestre, Peter Denes, A.L. Davi Kilcoyne, Stefano Marchesini, Howard Padmore, Tolek Tyliszczak, Tony Warwick, Xiaowen Shi, James Lee, Young-Sang Yu, Jordi Cabana, John Joseph, Harinaraya Krishnan, Talita Perciano, Filipe R. Maia, David A. Shapiro, Near-edge X-ray refraction fine structure microscopy, Appl. Phys. Lett. 110 (2017) 063101.
[33] M. Beckers, T. Senkbeil, T. Gorniak, M. Reese, K. Giewekemeyer, S.-C. Gleber, T. Salditt, A. Rosenhahn, Chemical contrast in soft X-ray ptychography, Phys. Rev. Lett. 107 (2011) 208101.
[34] J. Rodenburg, Ptychography and related diffractive imaging methods, Adv. Imaging Electron Phys. 150 (2008) 87–184.
[35] A.M. Maiden, J.M. Rodenburg, M.J. Humphry, Optical ptychography: A practical implementation with useful resolution, Opt. Lett. 35 (2010) 2585–2587.
[36] D.A. Muller, Z. Chen, Y. Jiang, M. Odstrcil, Yimo Han, P. Purohit, M.W. Tate, S. M. Gruner, V. Elser, Phase imaging beyond the diffraction limit with electron ptychography, Microsc. Microanal. 25 (2019) 6–7.
[37] A.R. Lupini, M.P. Oxley, S.V. Kalinin, Pushing the limits of electron ptychography, Science 362 (2018) 399–400.
[38] S. Baier, C.D. Damsgaard, M. Scholz, F. Benzi, A. Rochet, R. Hoppe, T. Scherer, J. Shi, A. Wittstock, B. Weinhausen, J.B. Wagner, In situ ptychography of heterogeneous catalysts using hard X-rays: high resolution imaging at ambient pressure and elevated temperature, Microsc. Microanal. 22 (2016) 178–188.
[39] K. Wakonig, A. Diaz, A. Bonnin, M. Stampanoni, A. Bergamaschi, J. Ihli, M. Guizar-Sicairos, A. Menzel, X-ray Fourier ptychography, Sci. Adv. 5 (2019) eaav0282.
[40] M.D. Seaberg, B. Zhang, D.F. Gardner, E.R. Shanblatt, M.M. Murnane, H. C. Kapteyn, D.E. Adams, Tabletop nanometer extreme ultraviolet imaging in an extended reflection mode using coherent Fresnel ptychography, Optica 1 (2014) 39–44.
[41] C. Jacobsen, S. Wirick, G. Flynn, C. Zimba, Soft X-ray spectroscopy from image sequences with sub-100 nm spatial resolution, J. Microsc. 197 (2000) 173–184.
[42] T. Sun, G. Sun, F. Yu, Y. Mao, R. Tai, X. Zhang, G. Shao, Z. Wang, J. Wang, J. Zhou, Soft X-ray ptychography chemical imaging of degradation in a composite surface-reconstructed Li-rich cathode, ACS Nano 15 (2020) 1475–1485.
[43] J. Lim, Y. Li, D.H. Alsem, H. So, S.C. Lee, P. Bai, D.A. Cogswell, X. Liu, N. Jin, Y. S. Yu, N.J. Salmon, Origin and hysteresis of lithium compositional spatiodynamics within battery primary particles, Science 353 (2016) 566–571.
[44] H.D. Deng, H. Zhao, N. Jin, L. Hughes, B.H. Savitzky, C. Ophus, D. Fraggedakis, A. Borbély, Y.-S. Yu, E.G. Lomeli, R. Yan, J. Liu, D.A. Shapiro, W. Cai, M.Z. Bazant, A.M. Minor, W.C. Chueh, Correlative image learning of chemo-mechanics in phase-transforming solids, Nat. Mater. 21 (2022) 547–556.
[45] H. Zhao, H.D. Deng, A.E. Cohen, J. Lim, Y. Li, D. Fraggedakis, B. Jiang, B.D. Storey, W.C. Chueh, R.D. Braatz, M.Z. Bazant, Learning heterogeneous reaction kinetics from X-ray videos pixel by pixel, Nature 621 (7978) (2023) 289–298.
[46] J. Wu, X. Zhu, M.M. West, T. Tyliszczak, H.W. Shiu, D. Shapiro, V. Berejnov, D. Susac, J. Stumper, A.P. Hitchcock, High-resolution imaging of polymer electrolyte membrane fuel cell cathode layers by soft X-ray spectro-ptychography, J. Phys. Chem. C 122 (2018) 11709–11719.
[47] P. Grosse, A. Yoon, C. Rettenmaier, A. Herzog, S.W. Chee, B. Roldan Cuenya, Dynamic transformation of cubic copper catalysts during CO_2 electroreduction and its impact on catalytic selectivity. Nat. Commun. 12 (2021) 6736.
[48] C. Zhang, J. Chen, H. Yuan, J. Wang, T. Sun, D. Higgins, A.P. Hitchcock, Atomically dispersed Ni-NC electrocatalysts, studied by Ni L-edge spectro-ptychography, J. Electron Spectrosc. Relat. Phenom. 266 (2023) 147364.
[49] C. Zhang, N. Mille, H. Eraky, S. Stanescu, S. Swaraj, R. Belkhou, D. Higgins, A. Hitchcock, Copper carbon dioxide reduction electrocatalysts studied by in-situ Soft X-ray spectro-ptychography, Cell Rep. Phys. Sci. 12 (2023) 101665.
[50] Victoria Savikhin, David A. Shapiro, Xiaodan Gu, Stefan D. Oosterhout, Michael F. Toney, Ptychography of organic thin films at soft X-ray energies, Chem. Mater. 31 (2019) 4913–4918.
[51] X. Zhu, A.P. Hitchcock, D.A. Bazylinski, P. Denes, J. Joseph, U. Lins, S. Marchesini, H.W. Shiu, T. Tyliszczak, D.A. Shapiro, Measuring spectroscopy and magnetism of extracted and intracellular magnetosomes using soft X-ray ptychography, Proc. Natl. Acad. Sci. USA *113* (51) (2016) E8219–E8227.
[52] H.N. Chapman, Fourth-generation light sources, IUCrJ 10 (3) (2023) 246–247.
[53] R. Belkhou, S. Stanescu, S. Swaraj, A. Besson, M. Ledoux, M. Hajlaoui, D. Dalle, HERMES: a soft X-ray beamline dedicated to X-ray microscopy, J. Synchrotron Radiat. 22 (2015) 968–979.
[54] K.V. Kaznatcheev, C. Karunakaran, U.D. Lanke, S.G. Urquhart, M. Obst, A. P. Hitchcock, Soft X-ray spectromicroscopy beamline at the CLS: Commissioning results, Nucl. Instrum. Methods Phys. Res. Sect. A: Accel., Spectrom. Detect. Assoc. Equip. 582 (2007) 96–99.
[55] A.P. Hitchcock, Analysis of X-ray images and spectra (aXis2000): a toolkit for the analysis of X-ray spectromicroscopy data, J. Electron. Spectrosc. Relat. Phenom. 266 (2023) 147360.
[56] I.N. Koprinarov, A.P. Hitchcock, C.T. McCrory, R.F. Childs, Quantitative mapping of structured polymeric systems using singular value decomposition analysis of soft X-ray images, J. Phys. Chem. B 106 (2002) 5358–5364.
[57] P. Jiang, D. Prendergast, F. Borondics, S. Porsgaard, L. Giovanetti, E. Pach, J. Newberg, H. Bluhm, F. Besenbacher, M. Salmeron, Experimental and theoretical investigation of the electronic structure of Cu_2O and CuO thin films on Cu (110) using x-ray photoelectron and absorption spectroscopy, J. Chem. Phys. 138 (2013) 024704.
[58] K. Desjardins, K. Medjoubi, M. Sacchi, H. Popescu, R. Gaudemer, R. Belkhou, N. Jaouen, Backside-illuminated scientific CMOS detector for soft X-ray resonant scattering and ptychography, J. Synchrotron Radiat. 27 (2020) 1577–1589.
[59] A.L.D. Kilcoyne, T. Tyliszczak, W.F. Steele, S. Fakra, P. Hitchcock, K. Franck, E. Anderson, B. Harteneck, E.G. Rightor, G.E. Mitchell, A.P. Hitchcock, Interferometer-controlled scanning transmission x-ray microscopes at the advanced light source, J. Synchrotron Radiat. 10 (2003) 125–136.
[60] N. Mille, H. Yuan, J. Vijayakumar, S. Stanescu, S. Swaraj, K. Desjardins, V. Favre-Nicolin, R. Belkhou, A.P. Hitchcock, Ptychography at the carbon K-edge, Commun. Mater. *3* (2022) 8.
[61] Hao Yuan, Hui Yuan, T. Casagrande, D. Shapiro, Y.-S. Yu, B. Enders, J.R.I. Lee, T. Van Buuren, M.M. Biener, St.A. Gammon, Th.F. Baumann, A.P. Hitchcock, 4D Imaging of ZnO-coated nanoporous Al_2O_3 aerogels by chemically-sensitive ptychographic tomography: implications for designer catalysts, ACS Appl. Nanomater. 4 (2021) 621–632.
[62] Z. Xu, C. Wang, H. Liu, Xi Tao, R. Tai, Low-dose, high-resolution and high-efficiency ptychography at STXM beamline of SSRF, J. Phys.: Conf. Ser. 849 (2017) 012033.
[63] Oliver Bunk, Martin Dierolf, S.øren Kynde, Ian Johnson, Othmar Marti, Franz Pfeiffer, Influence of the overlap parameter on the convergence of the ptychographical iterative engine, Ultramicroscopy 108 (2008) 481–487.
[64] Nicolas Burdet, Graeme R. Morrison, Xiaojing Huang, Xiaowen Shi, Jesse N. Clark, Fucai Zhang, Maria Civita, Ross Harder, Ian K. Robinson, Observations of artefacts in the x-ray ptychography method, Opt. Express 2 (2014) 10294–10303.
[65] V. Favre-Nicolin, G. Girard, S. Leake, J. Carnis, Y. Chushkin, J. Kieffer, M. I. Richard, PyNX: high-performance computing toolkit for coherent X-ray imaging based on operators, J. Appl. Crystallogr. 53 (2020) 1404–1413. Available at ⟨http://ftp.esrf.fr/pub/scisoft/PyNX/doc⟩.
[66] F. Zhang, I. Peterson, J. Vila-Comamala, A. Diaz, F. Berenguer, R. Bean, B. Chen, A. Menzel, I.K. Robinson, J.M. Rodenburg, Translation position determination in ptychographic coherent diffraction imaging, Opt. Express 21 (2013) 13592–13606.
[67] Xiaojing Huang, Hanfei Yan, Ross Harder, Yeukuang Hwu, Ian K. Robinson, Yong S. Chu, Optimization of overlap uniformness for ptychography, Opt. Express 22 (2014) 12634–12644.
[68] T. Sun, T. Zuo, S. He, B. Yuan, X. Li, G. Zhou, J. Abate, A, J. Wang, Ionic liquid functionalized tin halide perovskite investigated by STXM and spectro-ptychography, J. Electron Spectrosc. Rel. Phenom. 265 (2023) 147330.
[69] Wang, J., Radiation chemistry by soft X-ray spectromicroscopy, PhD thesis, McMaster University (2008).

[70] V. Berejnov, B. Rubinstein, L. Melo, A.P. Hitchcock, First principles X-ray absorption dose calculation for time dependent mass and optical density, J. Synchrotron Radiat. 25 (2018) 833–847.
[71] J. Wang, C. Morin, L. Li, A.P. Hitchcock, X. Zhang, T. Araki, A. Doran, A. Scholl, Radiation damage in soft X-ray microscopy, J. Electron Spectrosc. Rel. Phenom. 170 (2009) 25–36.
[72] Carles Bosch, Ana Diaz, Mirko Holler, Manuel Guizar-Sicairos, Tomas Aidukas, Alexandra Pacureanu, Elisabeth Müller, Christopher J. Peddie, Lucy Collinson, Yuxin Zhang, Andreas Menzel, Adrian A. Wanner, Andreas T. Schaefer, 3D-Imaging of synapses in neuronal tissues with synchrotron X-ray ptychography, bioRxiv 17 (2023), https://doi.org/10.1101/2023.11.16.567403 (Nov).
[73] D.A. Shapiro, S. Babin, S. Celestre, R.S. Chao, W. Conley, R.P. Denes, P. Enders, B. Enfedaque, P. James, S. Joseph, J.M. Krishnan, H. Marchesini, S. Muriki, K. Nowrouzi, K. Oh, S.R. Padmore, H. Warwick, T. Yang, L. Yashchuk, V.V. Yu, Y.-S. Zhao, J. An ultrahigh-resolution soft x-ray microscope for quantitative analysis of chemically heterogeneous nanomaterials, Sci. Adv. 6 (2020) eabc4904.
[74] B. Bozzini, G. Kourousias, A. Gianoncelli, M.W.M. Jones, G.A. Van Riessen, M. Kiskinova, Soft X-ray ptychography as a tool for in operando morphochemical studies of electrodeposition processes with nanometric lateral resolution, J. Electron Spectrosc. Relat. Phenom. 220 (2017) 147–155.
[75] G. Kourousias, B. Bozzini, M.W.M. Jones, G.A. Van Riessen, S. Dal Zilio, F. Billè, M. Kiskinova, A. Gianoncelli, Monitoring dynamic electrochemical processes with in situ ptychography, Appl. Nanosci. 8 (2018) 627–636.
[76] M. Kazemian, F. Rossi, A. Casaroli, T. Caielli, B. Kaulich, M. Kiskinova, I. Sgura, B. Bozzini, X-ray imaging and micro-spectroscopy unravel the role of zincate and zinc oxide in the cycling of zinc anodes in mildly acidic aqueous electrolytes, J. Power Sources 524 (2022) 231063.
[77] J. Vijayakumar, N. Mille, H. Yuan, S. Stenescu, S. Swaraj, K. Desjardins, F. Orsini, V. Favre-Nicolin, E. Najafi, A.P. Hitchcock, R. Belkhou, Soft X-ray spectro-ptychography of boron nitride nanobamboos, carbon nanotubes and permalloy nanorods, J. Synchrotron Radiat. 30 (2023) 746–757.
[78] T.D. Sowers, D. Adhikari, J. Wang, Y. Yang, D.L. Sparks, Spatial associations and chemical composition of organic carbon sequestered in Fe, Ca, and organic carbon ternary systems, Environ. Sci. Technol. 52 (2018) 6936–6944.
[79] M. Du, D. Gürsoy, C. Jacobsen, Near, far, wherever you are: Simulations on the dose efficiency of holographic and ptychographic coherent imaging, J. Appl. Crystallogr. 53 (2020) 748–759.
[80] F. Witwer, P. Modregger, Object initialization for ptychographic scans with reduced overlap, AIP Conf. Proc. 2990 (2023) (040005).
[81] E. Qoku, K. Xu, J. Li, P.J.M. Monteiro, K.E. Kurtis, Advances in imaging, scattering, spectroscopy, and machine learning-aided approaches for multiscale characterization of cementitious systems, Cem. Concr. Res. 174 (2023) 107335.
[82] M. Du, S. Kandel, J. Deng, X. Huang, A. Demortiere, T.T. Nguyen, R. Tucoulou, V. D. Andrade, Q. Jin, C. Jacobsen, Adorym: a multi-platform generic X-ray image reconstruction framework based on automatic differentiation, Opt. Express *29* (2021) 10000–10035.
[83] H. Chang, Z. Rong, P. Enfedaque, S. Marchesini, Iterative X-ray spectroscopic ptychography, J. Appl. Cryst. 53 (2020) 937–948.
[84] S. Liu, Z. Xu, Z. Xing, X. Zhang, R. Li, Z. Qin, Y. Wang, R. Tai, Periodic artifacts generation and suppression in X-ray ptychography, Photonics 10 (2023) 532.
[85] M. Odstrčil, M. Holler, M. Guizar-Sicairos, Arbitrary-path fly-scan ptychography, Opt. Express 26 (2018) 12585–12593.
[86] Maik Kahnt, Lukas Grote, Dennis Brückner, Martin Seyrich, Felix Wittwer, Dorota Koziej, Christian G. Schroer, Multi-slice ptychography enables high-resolution measurements in extended chemical reactors, Sci. Rep. 11 (2021) 1500.